

# Study the Effects of Pure Tin Oxide Nanoparticles Doped with Cu, Prepared by the Biosynthesis Method, on Bacterial Activity

Nada K. Abbas<sup>1</sup>  , Duha S. Shaker<sup>\*2</sup>  

<sup>1</sup>Department of Physics, College of Science for Women, University of Baghdad, Baghdad, Iraq

<sup>2</sup>Al-Karkh University of Science, Baghdad, Iraq

\*Corresponding Author.

Received 26/12/2022, Revised 26/09/2023, Accepted 28/09/2023, Published Online First 20/04/2024



© 2022 The Author(s). Published by College of Science for Women, University of Baghdad.

This is an Open Access article distributed under the terms of the [Creative Commons Attribution 4.0 International License](https://creativecommons.org/licenses/by/4.0/), which permits unrestricted use, distribution, and reproduction in any medium, provided the original work is properly cited.

## Abstract

In this study, pure SnO<sub>2</sub> nanoparticles were doped with 2% at wt. of copper by biosynthesis method. As raw materials, SnCl<sub>2</sub>·2H<sub>2</sub>O, CuCl<sub>2</sub>·2H<sub>2</sub>O, and ESM biomaterial were used as eggshell membranes. Samples were annealed at 550 °C for 3 h. The bacterial activity against E-coli Gram-negative and S. aureus Gram-positive strains and higher inhibition of concentrations in S.a-ureus was obtained from E-coli. The MIC method was used for the minimum inhibitory concentration. The results of XRD showed that the samples crystallized within the tetragonal rutile type and that the average crystal size is pure SnO<sub>2</sub> and SnO<sub>2</sub>: Cu (24.2, 16.6) nm respectively. SEM and AFM tests were also carried out. The UV-Vis studies revealed reflection spectroscopy at the energy gap of SnO<sub>2</sub>, and SnO<sub>2</sub>: Cu 2% is (4.30, 4.35) eV respectively. The AFM results showed the roughness rate of the prepared samples (6.34, 9.13) nm respectively. An EDX test was also performed for the prepared samples. The aim of the work is to create pure SnO<sub>2</sub> nanoparticles through active biosynthesis study the effect of doping it with Cu and study its effect on its structural and optical properties as well as how to use it as an antibacterial.

**Keywords:** ESM, E-coli & S. aureus, MIC method, SnO<sub>2</sub> biosynthesis, SnO<sub>2</sub>:Cu., Structure of SnO<sub>2</sub>.

## Introduction

SnO<sub>2</sub> is the least expensive and least toxic metal oxide nanoparticle. It is an n-type semiconductor with a 3.6 eV direct bandgap<sup>1</sup> Because of its unique physical and chemical properties, it has a wide range of applications in the fields of sensors<sup>2</sup>, optical electronics<sup>3</sup>, medicine<sup>4</sup>, and energy storage devices<sup>5</sup>. Because of two critical factors<sup>6</sup>: a) Increased surface area and b) Quantum effect, There are several methods for synthesizing and preparing tin oxide nanoparticles, including sol-gel<sup>7</sup>, solvothermal<sup>8</sup>, pulsed laser deposition<sup>9</sup>, chemical precipitation<sup>10</sup>, and green synthesis<sup>11</sup>. SnO<sub>2</sub> NPS has been developed because it is less expensive and

non-toxic. Tin oxide is an important material for the following reasons: It has a high degree of transparency in the visible spectrum, strong chemical and physical interaction with the absorbent species, Low operating temperature, strongly thermally stable in air up to 500 °C<sup>12</sup>.

The most readily available vital waste whereas the eggshell membrane ESM within the eggshell contains collagen proteins containing various amino acids, glycine, and alanine, Uronic acid contains many amino acids, carboxylates, carbonyls, and aldehyde functional groups<sup>13</sup>, where they act as reducing agents to form a nano-metal oxide, and the

ESM model was used in this case because SnO<sub>2</sub> nanoparticles are assembled using natural biosynthesis rather than toxic chemicals. It appears that the use of ESM is appropriate for medical and antibacterial applications. Mataji Palaz discussed the morphology and functional groups of ESM, as well as the field applications of their systems<sup>14</sup>. Chang et al.<sup>15</sup>. Gold nanocomposites using ESM and studying their bio-properties. Wang et al.<sup>16</sup>.

## Materials and Methods

### Materials:

SnCl<sub>2</sub>.2H<sub>2</sub>O company Qualikems (India), CuCl<sub>2</sub>.2H<sub>2</sub>O CDH, India), Deionized water (Local, Iraq), Eggshell membrane ESM Local by hand, Iraq). For preparation of SnO<sub>2</sub> NPS pure and 2% Cu

### Preparation of pure SnO<sub>2</sub> and doped with Cu nanoparticles by using ESM as bioactivity

Pure tin oxide nanoparticles were prepared and doped with Cu by biosynthesis method using an eggshell membrane ESM. 1g of SnCl<sub>2</sub>.2H<sub>2</sub>O was taken and dissolved in 25 ml of deionized water and stirred for 1 hour for complete dissolution and homogeneity, then ESM was added at 0.25g for 24 hours. The eggshell membrane was filtered and washed to separate the unwanted components. At 550 °C for 3 days, the ESM changed color from pale yellow to brown, and pure SnO<sub>2</sub> NPs were obtained. Preparation of pure nano-tin oxide doped with Cu. CuCl<sub>2</sub>.2H<sub>2</sub>O was doped by 2% in addition to being doped by 1.12 g of SnCl<sub>2</sub>.2H<sub>2</sub>O and 50 ml of water, according to equation<sup>19</sup>:

$$\% \text{ dopants} = \frac{M \text{ dopants}(x) \text{ molarity}}{M \text{ dopants} + M \text{ origin}} \dots\dots 1$$

M dopants(x): The molar concentration doped CuCl<sub>2</sub>.2H<sub>2</sub>O. % dopants: doped concentrations. M origin: The molar concentration of the original material SnCl<sub>2</sub>.2H<sub>2</sub>O.

Where molarity is given by relation<sup>20</sup>:

$$M = \frac{W}{m.Wt} \times \frac{1000}{V} \dots\dots 2$$

V: The volume of deionized water, W: the weight, m.Wt: Molecular weight.

obtained nano carbonate with ESM and studied its fluorescent application. Also, SnO<sub>2</sub> NPS was prepared and studied pure and doped with Cu, as copper has high electrical and thermal conductivity and is the most conductive mineral for electricity and heat after silver<sup>17,18</sup>. The study aims to form pure SnO<sub>2</sub> nanoparticles doped with Cu by active biosynthesis and use the prepared materials for medical applications

It was placed on stirring for 1 hour, then weighted 0.5 g of ESM and put in the solution for 24 hours, then separated the unwanted materials and washed the substance in deionized water and ethanol, then annealed the precipitate at 550 °C for 3 hours.

### Determination of the effect of bacterial activity of prepared nanoparticles

### Determination of the effect of antibacterial activity of SnO<sub>2</sub> and SnO<sub>2</sub>: Cu NPs by Well Diffusion assay.

The medium Mueller Hinton agar was prepared in accordance with the instructions. company's instructions prepared for the medium, dissolved in a specified amount of D.W., and entered into an autoclave at a temperature of 121°C and pressure at 15 pounds/inch<sup>2</sup> for 15 minutes. It was poured into Petri dishes.

The bacteria to be measured were placed in dishes and then refrigerated at 4 °C. The effect of the prepared substance was spread on it, and the bacteria Four different types of bacteria were tested for activity. There are two types of gram-positive and gram-negative of SnO<sub>2</sub> Pure and SnO<sub>2</sub>:Cu NPs are prepared by using ESM, The wells were made inside the Petri dish, and the material was placed in the wells. The Petri agar was incubated in an incubator at 37°C for 24 hours. The bacteria were local isolates that were activated by nutrients. agar and used in the assays. If bacterial growth extends to the nanoparticle-containing well, the bacterial strain is considered resistant to the nanoparticles. If there is this indicates that the nanoparticle has cleared the area around the antibiotic well. harmed the bacteria. to determine whether a bacterial strain is sensitive to an antibiotic, the size of the inhibition

zone can be measured and compared. to control well <sup>21</sup>.

### Determine the Minimum inhibitor concentration MIC as the Antibacterial activity of SnO<sub>2</sub> pure and doped with Cu Nanoparticle.

The antibacterial activity of SnO<sub>2</sub> was measured, and SnO<sub>2</sub>:Cu 2% of the nanoparticles were then evaluated against gram-positive bacteria. Staphylococcus aureus and gram-negative bacteria Escherichia coli by serial dilution by determining the minimum inhibitory concentration MIC in the cultural broth. 0.7 mL of the medium was taken in a test tube. 0.7ml of The test substance was added to the tube. 70 µl of the bacterial strains E-Coli, and S. aureus, and the serial dilution was performed at five concentrations. 50%, 25%, 12.5%, 6.25, and 3.125% of SnO<sub>2</sub> nanoparticles were obtained from the Eggshell membrane ESM at a stock concentration of 0.25 g/ml SnO<sub>2</sub> The control was

## Results and Discussion

### XRD Analysis

The XRD pattern of pure SnO<sub>2</sub> doped with 2% at wt. of Cu nanoparticles and annealed at 550 °C for 3 hours is shown in Fig 1. All samples were identified as tetragonal rutile, and the results are in agreement with JCPDS standard card No. (96-900-9083) where the diffraction peaks coincide with the standard data from (110), (101), and (211), and the most obvious peak is (110). There are no identical peaks for Cu The results match those of the researchers Sagadevan et al., <sup>22</sup>, and this leads to the conclusion that there are two types of doped SnO<sub>2</sub> with Cu: substitutive and interstitial. In this case, some ions are replaced by Sn + with a Cu + ion based on similar radius Sn, Cu (0.69,0.73) Å, respectively. The average grain size of the nanoparticles was calculated based on Scherrer's equation <sup>23</sup>.

$$d = \frac{\kappa\lambda}{\beta\cos\theta} \dots\dots\dots 3.$$

d: is the mean crystalline size, K is the constant = 0.89, λ is the wavelength of the incident beam λ=1.5418Å CuKα, β is the full-width for a half maximum is the Bragg diffraction angle in degrees. It was found that the average crystal size as shown

SnO<sub>2</sub>:Cu NPs obtained from ESM 0.25, 0.5 g. tubes unexposed. All samples were incubated for 24 hours at 37 °C.

### Characterization

The X-ray diffraction XRD pattern of tin oxide nanoparticles was recorded by Card No.96-900-9083 using CuKα,λ=0.154 nm. The particle morphology and size were examined by scanning electron microscopy SEM ZEISS model Sigma VP with a magnification of 50.00KX and EDX Oxford instruments in the UK. Optical properties were analyzed using ultraviolet diffusion. Reflection Spectroscopy with UV-VIS Shimadzu within the wavelength range of 280 nm-900nm. The AFM revealed the shape of SnO<sub>2</sub> NPs in the DME Denmark model, and the cumulative distribution plot revealed the average grain

in Tab. 1, for pure SnO<sub>2</sub> is 24.2nm and for the doped with 2%at wt of Cu16.60 nm. The presence of doping reduces the crystal size, which means that the presence of copper ions in SnO<sub>2</sub> hinders the growth of crystal grains. From the figure, we notice that with the presence of copper ions, the intensity of the XRD peaks increases, which indicates that the doping increases crystallinity.

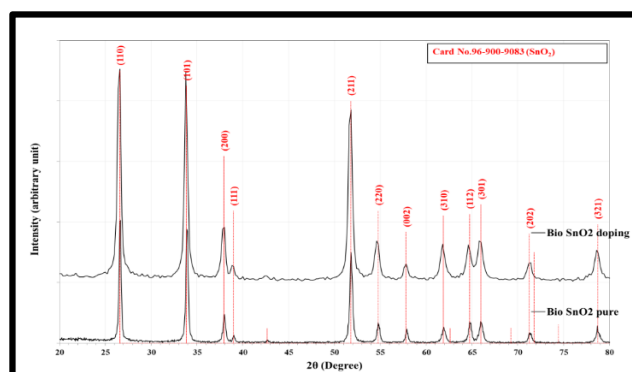


Figure 1. X-ray diffraction pattern of a) pure SnO<sub>2</sub> nanoparticles .b) SnO<sub>2</sub> NPS doped with Cu 2%

**Table 1. the grain size of the pure and doped nanoparticles**

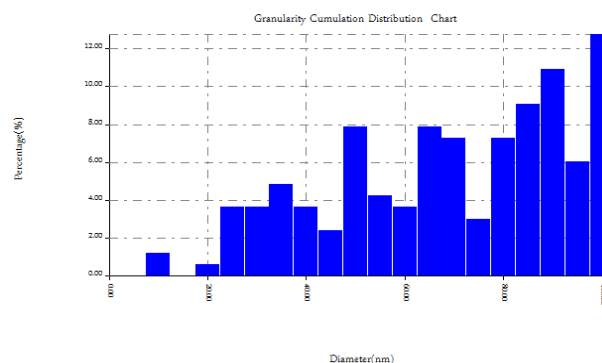
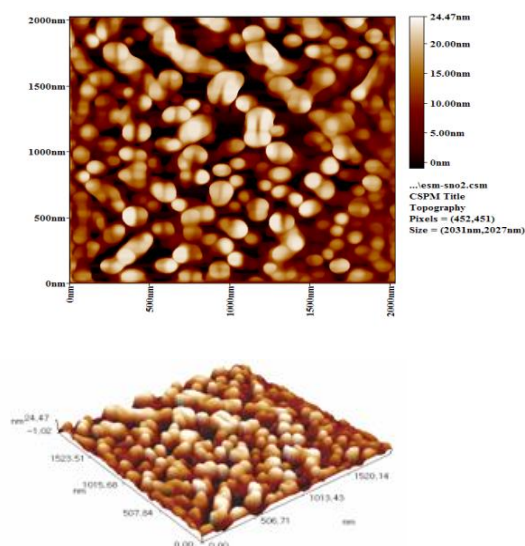
Cu%	G.S (nm)
0	<b>24.2</b>
2	<b>16.60</b>

## AFM Examination

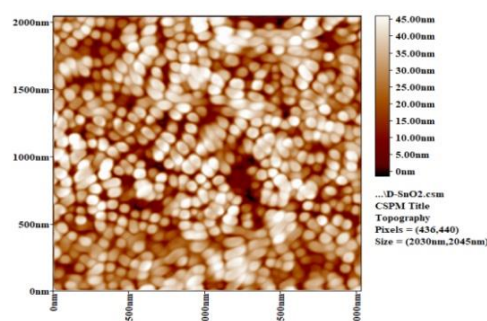
Fig 2 shows an atomic force microscope image of the pure SnO<sub>2</sub> sample surface and SnO<sub>2</sub> doped with 2% at wt. of Cu and annealed at 550 °C prepared in a bio-based method. The 2D and 3D images show that the SnO<sub>2</sub> topography for all samples has spherical shapes as shown in Fig 2. Moreover, in the area that has been investigated by AFM, it is found that the roughness average of pure SnO<sub>2</sub> NPS and SnO<sub>2</sub>:Cu at 550 °C annealing are 6.34 nm and 9.13 nm, while the grain size is 66.9 nm and 67.4 nm, respectively. The grain size increased in doped samples because crystallinity defects occurred, which leads to an increase in the size due to the addition of Cu, as well as increasing roughness, as shown in Table 2

**Table 2. The grain size and roughness of pure SnO<sub>2</sub> nanoparticles doped with Cu, annealing at 550°C**

Cu doping concentration W%	average size (nm)	Roughness (nm)	RMS
0	<b>66.9</b>	<b>6.34</b>	<b>7.31</b>
2	<b>67.4</b>	<b>9.13</b>	<b>11</b>



(A)



(B)

Figure 2. The AFM of (A): pure SnO<sub>2</sub> Nano nanoparticles in 2D and 3D and Granularity Cumulation Distribution Report, and (B) SnO<sub>2</sub>: Cu in 2D and 3D and Granularity Cumulation Distribution Report, annealing at 550°C.

## SEM Scan Results

By examining SEM images of pure SnO<sub>2</sub> and SnO<sub>2</sub>:Cu samples at 2% wt concentration and annealing at 550°C prepared by biosynthesis using eggshell membrane as shown in Fig 3, the form and size of the grains can be determined. Since the SEM images give clarity about the surface morphology and the average particle size shown in this figure for the pure SnO<sub>2</sub> is 68.02nm and for SnO<sub>2</sub>:Cu is 100 nm which proves that the prepared samples are within the nanoscale domain <sup>24</sup>.

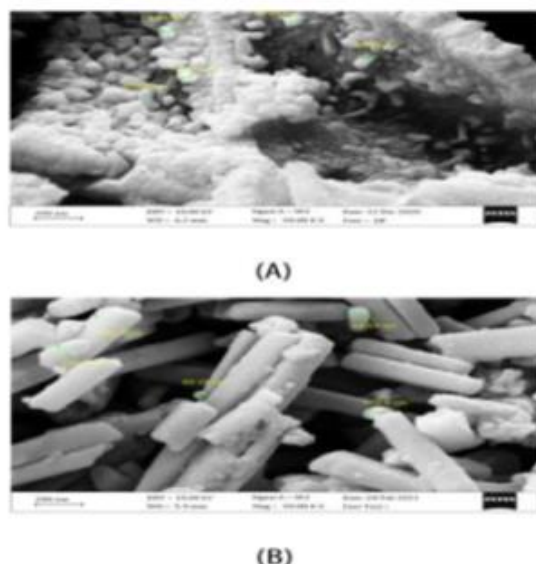


**Figure 3. SEM images of (A): pure SnO<sub>2</sub> at 550°C annealing temperature, (b): SnO<sub>2</sub>: Cu at 550°C annealing temperature.**

## EDX Results

EDX describes the elemental composition in the as-prepared samples (SnO<sub>2</sub> and SnO<sub>2</sub>:Cu) and that Cu ions were successfully incorporated into the SnO<sub>2</sub> lattice. These nanoparticles have spherical forms and are less than 100 nm in size. The EDX results are shown in Fig 4, which shows the rising peaks representing the quantity of Sn, O, Cu, and C. The C element is present in the eggshell membrane because it contains carbonyl and carboxyl which contain element C. The actual composition of the rated EDX- prepared materials is scheduled in Table 3 below:

**Table 3. The actual composition of the rated EDX- prepared materials is scheduled**

EDXComposition	Sn (wt%)	O(wt%)	Cu(wt%)	C(wt%)
pure	89.4	8.9	0	1.7
2% Cu	0.1	2.5	44.8	9.8

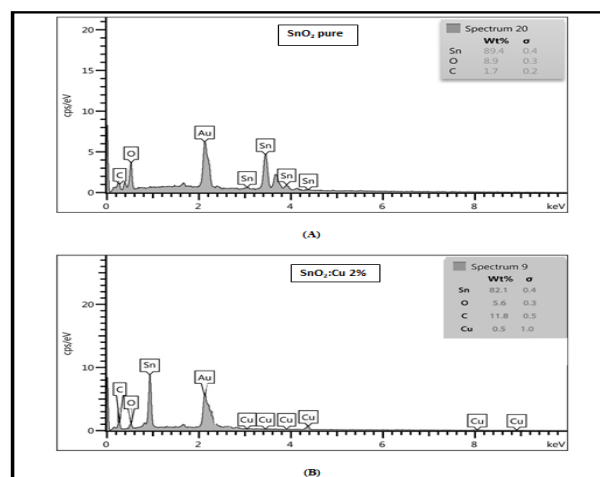


**Figure 4. EDX image of. A) Pure SnO<sub>2</sub>. B) SnO<sub>2</sub>: 2% Cu**

## Optical Studies

In order to better understand the effect of copper doping on the optical properties of SnO<sub>2</sub> nanoparticles, This UV-VIS spectroscopy analysis was performed. Fig 5, shows the variation in absorbance with wavelength within the range of 280nm-900nm for the pure SnO<sub>2</sub> samples and those doped with Cu ions as shown in Tab.4, where the band gap is calculated using the Planck equation <sup>25</sup>.

$$E = \frac{1240}{\lambda} \text{ ev} \dots\dots 4.$$

The absorbance decreases as the wavelength increases. This means that the incident photon is unable to excite the electron and transfer it from the valence to the conduction band, because its energy is less than the energy gap's value <sup>26</sup>. Table 4 shows the values of the energy gap for the permissible direct transmission of the pure and 2%wt doped SnO<sub>2</sub> nanoparticles. The values of the energy gap increase with doping and the reason for that is due to the fact that the doping leads to reducing the dangling bonds, filling voids, and reducing defects that are formed during the preparation process.

**Table 4. of the energy band gap for pure and doped nanoparticle concentrations with Cu**

Concentration ratios%	Cu	Band gap (Eg)	wave length ( $\lambda$ ) nm
0		4.30	288
2		4.35	285

It is known that semiconducting nanoparticles have a distinct absorption edge and that shifting the material to the nanoscale leads to its deviation towards short wavelengths. The pure SnO<sub>2</sub> nanoparticles should have a wide energy gap due to the quantum confinement of the electron gap pair formed as a result of photon absorption of energy. The slight increase in the energy gap after doping with Cu is the result of a slight decrease in the crystal grain size, this was given by the interpretation of the XRD results, where a slight blueshift was observed for these peaks, indicating a decrease in the energy gap. Also, this slight improvement in optical range difference with an increase of Cu concentration by 2% may be due to the presence of grid defects or stacking errors.

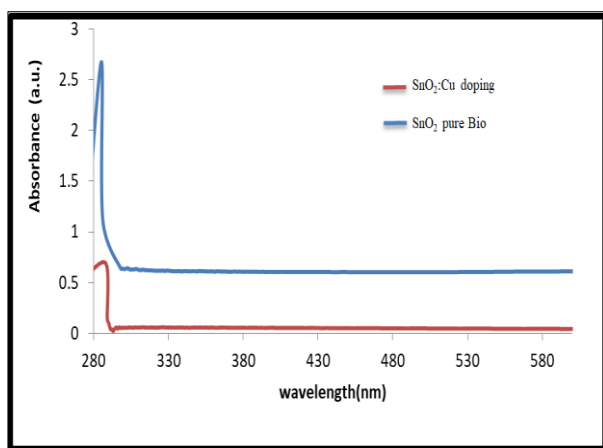


**Figure 5. Shows the absorbance spectrum of pure SnO<sub>2</sub> NPs& doped with Cu.**

#### Fourier Transform Infra-Red spectroscopy (FTIR)

This procedure has been carried out in order to pinpoint the biomolecules and reduction compounds in charge of producing the SnO<sub>2</sub> NPs produced by the eggshell membrane. Fig 6 shows the FTIR spectrum for SnO<sub>2</sub> NPs. The bands at 34093cm<sup>-1</sup>

are given to the O-H and N-H stretching vibration of phenols and proteins from the eggshell membrane M.Buck<sup>27</sup>. Other peaks at 1364 cm<sup>-1</sup> represent to C-H stretch of alkanes Elzbieta Drzymala<sup>28</sup>. Peaks at 1631\_1633cm<sup>-1</sup> were identified as belonging to the O-H bending mode in the protein's characteristic amine I group. The Peak at 1223cm<sup>-1</sup> represents C-O Phenol, Peak at 1714cm<sup>-1</sup> represents C=O Fan Liu\*, Yu Liu, Jia Chuan Chen, Zhen Wang<sup>29</sup>, while the peak at 623 – 619 cm<sup>-1</sup> region corresponds to the stretching modes of the Antisymmetric Sn-O-Sn Yang et. Al<sup>30</sup>. These bands are characteristic of Sn- OH terminal bonds of the SnO<sub>2</sub> crystalline phase at 1110\_1114cm<sup>-1</sup> <sup>31</sup>.

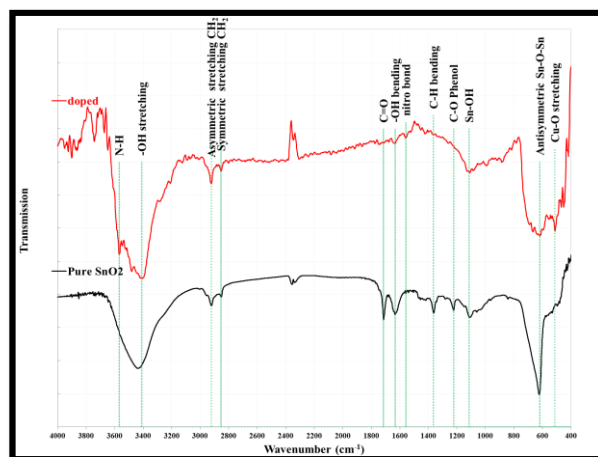


**Figure 6. FTIR spectra of pure tin oxide nanoparticles synthesized by active biosynthesis using eggshell membrane**

#### Anti-bacterial activity of SnO<sub>2</sub> NPs pure and doped with Cu

Biosynthesis of SnO<sub>2</sub> NPs showed excellent antibacterial activity against multiple bacterial pathogens by Petri-agar methods, such as Gram-positive bacteria *Staphylococcus aureus*, *Streptococcus pyogenes*, and Gram-negative bacteria *Escherichia coli*, *Pseudomonas aeruginosa*, as obtained from the eggshell membrane ESM, as shown in Fig 7 The diameter of the inhibitory zone varies. The results showed that *Pseudomonas aeruginosa* occupied greater inhibition areas than *Staphylococcus aureus* compared to *Escherichia coli* and *Streptococcus pyogenes*, which could be due to differences in cell wall composition. The

diameter of the inhibition zone was 37 mm, the highest inhibition area for all bacterial pathogens. The reason is that it has an effect on the metabolism of bacteria as an enzyme inhibitor, and that  $\text{SnO}_2$  Pure has no inhibition zone, unlike *S. aureus* bacteria. where the outer membrane of the bacteria provides a strong interaction with the prepared samples and the presence of Sn enhances the substance and the association of NPs with the bacteria and thus the bactericidal activity<sup>32</sup> and the doping area of the material is higher than pure because the particle size is smaller in the doped than in the pure<sup>33</sup>. The experiment was conducted under aerobic conditions at a temp of 37°C.

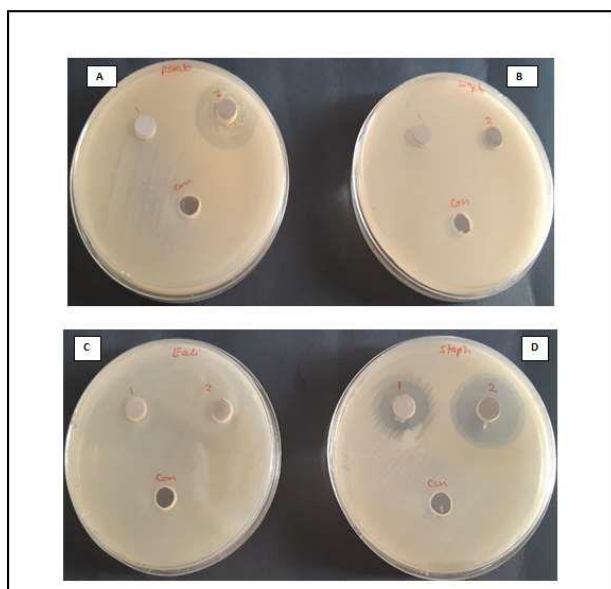


**Figure 7. Antibacterial activity of 1)  $\text{SnO}_2$  NPs, 2)  $\text{SnO}_2$ :Cu 2% from ESM for bacterial strains.**

**A) *Pseudomonas aeruginosa*, B) *Streptococcus pyogenes*, C) *E. coli*, D) *S. aureus*.**

this study the *Escherichia coli* strain as well as *Staphylococcus aureus* were used for the ESM biomaterial. It can be seen that *Staphylococcus aureus* disrupted the formation of peptide cross-links to the cell wall more than *E. coli* for different

## Conclusion

A simple, economical, and environmentally friendly route has been developed for the synthesis of  $\text{SnO}_2$  nanoparticles using an active biosynthesis method using an eggshell membrane. Crystal size was

calculated by XRD data of nanoparticles using, and nanoparticle size was measured from SEM data obtained from nanoparticle size. Shows the XRD pattern. The tin oxide nanoparticles formed from concentrations of the substance 50%, 25%, 12.5%, 6.25%, 3.125% respectively of the pure substance and doped with Cu. Whereas, in the *E. coli* strain, complete inhibition was obtained in pure  $\text{SnO}_2$  at a concentration of only 50%, while  $\text{SnO}_2$ :Cu was inhibited at concentrations 12.5%, 25%, and 50% only. As for the *Staphylococcus aureus* strain, pure  $\text{SnO}_2$  was inhibited at a concentration of only 50%, and  $\text{SnO}_2$ :Cu was inhibited for all concentrations of 3.125%, 6.25%, 12.5%, 25%, and 50%, respectively. The reason for this is that the peptides in the *S. aureus* strain interact with  $\text{Sn}^{+2}$  ions and direct the growth of  $\text{SnO}_2$  nanoparticles<sup>34</sup> as shown in Fig 8, so these peptides can achieve an easy interaction environment as they ensure biocompatibility. The major part of *S. aureus* is built of interconnected glycan-oligopeptide chains, and glycan strings are interconnected by parallel, shell-like layers<sup>35</sup>. The cells of *Escherichia coli* are surrounded by a complex cell wall consisting of two concentric lipid bilayers, the outer membrane, and the cytoplasmic membrane with a circumferential space between them<sup>36</sup>. The outer membrane is filled with lipopolysaccharides connected with complex lipids with fatty acid tails, and the space between the membranes is filled with peptidoglycan and a group of small soluble proteins. *E. coli* cell wall thickness and Gram-negative bacteria are 4nm<sup>37</sup>.

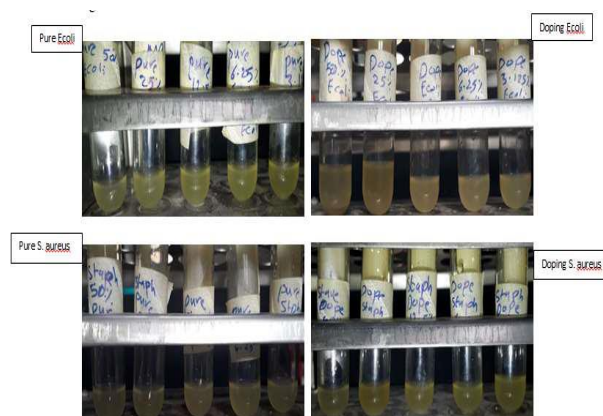


**Figure 8. Bacterial activity by MIC for different concentrations of pure  $\text{SnO}_2$  &  $\text{SnO}_2$ :Cu**

calculated by XRD data of nanoparticles using, and nanoparticle size was measured from SEM data obtained from nanoparticle size. Shows the XRD pattern. The tin oxide nanoparticles formed from

this structure are tetragonal crystals, and the crystal size is 24.2nm, and 16.60nm for the pure samples and doped with 2 wt% Cu respectively. AFM results showed that the size of the granules inside the nanoscale is spherical in different sizes ranging from 66.9nm to 67.4nm. The highest roughness is 9.13 nm for the sample doped with 2% Cu. The roughness of the pure samples is 6.34 nm.

This method by which SnO<sub>2</sub> nanoparticles are obtained is environment-friendly for commercial production as it does not involve the use of

### Authors' Declaration

- Conflicts of Interest: None.  
- We hereby confirm that all the Figures and Tables in the manuscript are ours. Furthermore, any Figures and images, that are not ours, have been included with the necessary permission for re-publication, which is attached to the manuscript.

### Authors' Contribution Statement

N. K. A. proposed the idea of research and guidance in how to prepare, as well as preparing the workplace. D. S. Sh. worked on preparing samples and conducting tests for them and verified the

### Journal Declaration:

N. K. A. is an Editor for the journal but did not participate in the peer review process other than as

hazardous and toxic sealing agents. Moreover, the concentration of the capping agent has a significant effect and can be seen in the crystal size, and a shift was seen in  $\lambda$  max.

Also, from the compositional results, energy gap values, absorbance increase, roughness, and other results obtained, it is clear that the prepared samples can be used in different applications such as solar cells, gas sensors, and different medical applications such as cancer and as an antibacterial activity to inhibit the action of bacteria.

- No animal studies are present in the manuscript.  
- No human studies are present in the manuscript.  
- Ethical Clearance: The project was approved by the local ethical committee in Al-Karkh University of Science, Baghdad, Iraq.

analytical methods. N. K. A. investigated and supervised the findings of this work. All authors discussed the results and contributed to the final manuscript

an author. The authors declare no other conflict of interest.

### References

1. Abdelkader E, Nadjia L, Naceur B, Noureddine B. SnO<sub>2</sub> foam grain-shaped nanoparticles: Synthesis, characterization and UVA light induced photocatalysis. *J Alloys Compd.* 2016; 679: 408–19. <https://doi.org/10.1016/j.jallcom.2016.04.016>
2. Sharma A, Ahmed A, Singh A, Oruganti S, Khosla A, Arya S. Recent advances in tin oxide nanomaterials as electrochemical/chemiresistive sensors. *J Electrochem Soc.* 2021; 168-2. <https://doi.org/10.1149/1945-7111/abdee8>
3. Chand P. Effect of pH values on the structural, optical and electrical properties of SnO<sub>2</sub> nanostructures. *Optik (Stuttg).* 2019; 181: 768–78. <https://doi.org/10.1016/j.ijleo.2018.10.203>
4. Sharma D, Kumar N, Mehrotra T, Pervaiz N, Agrawal L, Tripathi S, et al. In vitro and in silico molecular docking studies of Rheum emodi-derived diamagnetic SnO<sub>2</sub> nanoparticles and their cytotoxic effects against breast cancer. *New J Chem.* 2021; 45(3): 1695–711. <https://doi.org/10.1039/D0NJ04670A>
5. Suthakaran S, Dhanapandian S, Krishnakumar N, Ponpandian N. Hydrothermal synthesis of surfactant assisted Zn doped SnO<sub>2</sub> nanoparticles with enhanced photocatalytic performance and energy storage performance. *J Phys Chem Solids.* 2020; 141: 109407. <https://doi.org/10.1016/j.jpcs.2020.109407>
6. Zhu Q-L, Xu Q. Immobilization of ultrafine metal nanoparticles to high-surface-area materials and their catalytic applications. *Chem.* 2016; 1(2): 220–45. <https://doi.org/10.1016/j.chempr.2016.07.005>
7. Das I, Sagadevan S, Chowdhury ZZ, Hoque ME. Development, optimization and characterization of a two step sol-gel synthesis route for ZnO/SnO<sub>2</sub>

- nanocomposite. *J Mater Sci Mater Electron*. 2018; 29(5): 4128–35. <https://doi.org/10.1007/s10854-017-8357-5>
8. Jiang H, Wang R, Wang D, Hong X, Yang S. SnO<sub>2</sub>/diatomite composite prepared by solvothermal reaction for low-cost photocatalysts. *Catalysts*. 2019; 9(12): 1060. <https://doi.org/10.3390/catal9121060>
9. Zhang J, Chaker M, Ma D. Pulsed laser ablation based synthesis of colloidal metal nanoparticles for catalytic applications. *J Colloid Interface Sci*. 2017; 489: 138–49. <https://doi.org/10.1016/j.jcis.2016.07.050>
10. Arularasu M V, Anbarasu M, Poovaragan S, Sundaram R, Kanimozhi K, Magdalane CM, et al. Structural, optical, morphological and microbial studies on SnO<sub>2</sub> nanoparticles prepared by co-precipitation method. *J Nanosci Nanotechnol*. 2018; 18(5): 3511–7. <https://doi.org/10.1166/jnn.2018.14658>
11. Luque PA, Nava O, Soto-Robles CA, Chinchillas-Chinchillas MJ, Garrafa-Galvez HE, Baez-Lopez YA, et al. Improved photocatalytic efficiency of SnO<sub>2</sub> nanoparticles through green synthesis. *Optik (Stuttg)*. 2020; 206: 164299. <https://doi.org/10.1016/j.ijleo.2020.164299>
12. Pascariu P, Airinei A, Olaru N, Petrilă I, Nica V, Sacarescu L, et al. Microstructure, electrical and humidity sensor properties of electrospun NiO–SnO<sub>2</sub> nanofibers. *Sensors Actuators B Chem*. 2016; 222: 1024–31. <https://doi.org/10.1016/j.snb.2015.09.051>
13. Devi PS, Banerjee S, Chowdhury SR, Kumar GS. Eggshell membrane: a natural biotemplate to synthesize fluorescent gold nanoparticles. *RSC Adv*. 2012; 2(30): 11578–85. <https://doi.org/10.1039/C2RA21053C>
14. Baláz M. Eggshell membrane biomaterial as a platform for applications in materials science. *Acta Biomater*. 2014; 10(9): 3827–43. <https://doi.org/10.1016/j.actbio.2014.03.020>
15. Chang B, Qian L, Yuan H, Xiao D, Yang X, Paau MC, et al. Preparation of gold nanoparticles on eggshell membrane and their biosensing application. *Talanta*. 2010; 82(1): 177–83. <https://doi.org/10.1016/j.talanta.2010.04.014>
16. Wang Q, Liu X, Zhang L, Lv Y. Microwave-assisted synthesis of carbon nanodots through an eggshell membrane and their fluorescent application. *Analyst*. 2012; 137(22): 5392–7. <https://doi.org/10.1039/C2AN36059D>
17. Abbas NK, Shanan ZJ, Mohammed TH. Physical properties of Cu doped ZnO nanocrystalline thin films. *Baghdad Sci J*. 2022; 19(1): 217. <https://doi.org/10.21123/bsj.2022.19.1.0217>
18. Shaker DS, Abass NK, Ulwall RA. Preparation and study of the Structural, Morphological and Optical properties of pure Tin Oxide Nanoparticle doped with Cu. *Baghdad Sci J*. 2022; 19(3): 660. <https://doi.org/10.21123/bsj.2022.19.3.0660>
19. Muliyadi L, Doyan A, Susilawati S, Hakim S. Synthesis of SnO<sub>2</sub> Thin Layer with a Doping Fluorine by Sol-Gel Spin Coating Method. *J Penelit Pendidik IPA*. 2019; 5(2): 175–8. <https://doi.org/10.29303/jppipa.v5i2.257>
20. Mohammed A, Bachtar D, Siregar JP, Rejab MRM. Effect of sodium hydroxide on the tensile properties of sugar palm fibre reinforced thermoplastic polyurethane composites. *J Mech Eng Sci*. 2016; 10(1): 1765–77. <http://dx.doi.org/10.15282/jmes.10.1.2016.2.0170>
21. Brown DF, Kothari D. Comparison of antibiotic discs from different sources. *J Clin Pathol*. 1975; 28(10): 779–83. <http://dx.doi.org/10.1136/jcp.28.10.779>
22. Sagadevan S, Johan M, Bin R, Aziz FA, Hsu H-L, Selvin R, et al. Influence of Mn Doping on the Properties of Tin Oxide Nanoparticles Prepared by Co-Precipitation Method. *J Nanoelectron Optoelectron*. 2019; 14(4): 583–92. <https://doi.org/10.1166/jno.2019.2588>
23. Ehsani M, Hamidon MN, Toudeshki A, Abadi MHS, Rezaeian S. CO<sub>2</sub> gas sensing properties of screen-printed La<sub>2</sub>O<sub>3</sub>/SnO<sub>2</sub> thick film. *IEEE Sens J*. 2016; 16(18): 6839–45. <https://doi.org/10.1109/JSEN.2016.2587779>
24. Mohamed MB, Abdel-Kader MH. Effect of annealed ZnS nanoparticles on the structural and optical properties of PVA polymer nanocomposite. *Mater Chem Phys*. 2020; 241: 122285. <https://doi.org/10.1016/j.matchemphys.2019.122285>
25. Shamaila S, Bano T, Sajjad AKL. Efficient visible light magnetic modified iron oxide photocatalysts. *Ceram Int*. 2017; 43(17): 14672–7. <https://doi.org/10.1016/j.ceramint.2017.07.193>
26. Sagar P, Shishodia PK, Mehra RM, Okada H, Wakahara A, Yoshida A. Photoluminescence and absorption in sol-gel-derived ZnO films. *J Lumin*. 2007; 126(2): 800–806, 2007. <https://doi.org/10.1016/j.rinp.2013.11.001>
27. Buck M. Ab initio calculations of vibrational spectra of 2-methoxy ethanol in the C–H stretching range. *Phys Chem Chem Phys*. 2003; 5(1): 18–25. <https://doi.org/10.1039/B209917A>
28. Drzymała E, Gruzeł G, Depciuch J, Budziak A, Kowal A, Parlinska-Wojtan M. Structural, chemical and optical properties of SnO<sub>2</sub> NPs obtained by three different synthesis routes. *J Phys Chem Solids*. 2017; 107: 100–7. <https://doi.org/10.1016/j.jpcs.2017.03.026>

29. Liu F, Liu Y, Chen JC, Wang Z. FTIR Analysis of the Lignin Structure Changes of APMP Treated by Laccase and Laccase/Mediator System. *Adv Mat Res*. 2013; 734-737: 2089–93. <https://doi.org/10.4028/www.scientific.net/AMR.734-737.2089>
30. Yang H, Hu Y, Tang A, Jin S, Qiu G. Synthesis of tin oxide nanoparticles by mechanochemical reaction. *J Alloys Compd*. 2004; 363(1–2): 276–9. [https://doi.org/10.1016/S0925-8388\(03\)00473-0](https://doi.org/10.1016/S0925-8388(03)00473-0)
31. Singh AV, Jahnke T, Xiao Y, Wang S, Yu Y, David H, et al. Peptide-induced biomineralization of tin oxide (SnO<sub>2</sub>) nanoparticles for antibacterial applications. *J Nanosci Nanotechnol*. 2019; 19(9): 5674–86. <https://doi.org/10.1166/jnn.2019.16645>
32. Kasap SO, Rowlands JA. Direct-conversion flat-panel X-ray image detectors. *IEE Proceedings-Circuits, Devices Syst*. 2002; 149(2): 85–96. <https://doi.org/10.1049/ip-cds:20020350>
33. Kadhimi HT. Study of the Effect of Thickness and Annealing Process on Optical Properties of (SnO<sub>2</sub>: 5% Cu) Thin Films. *Al-Qadisiyah J Pure Sci*. 2013; 18(2): 113–27.
34. Amininezhad SM, Rezvani A, Amouheidari M, Amininejad SM, Rakhshani S. The antibacterial activity of SnO<sub>2</sub> nanoparticles against *Escherichia coli* and *Staphylococcus aureus*. *Zahedan J Res Med Sci*. 2015; 17(9). <https://doi.org/10.17795/zjrms-1053>
35. Yao X, Jericho M, Pink D, Beveridge T. Thickness and elasticity of gram-negative murein sacculi measured by atomic force microscopy. *J Bacteriol*. 1999; 181(22): 6865–75. <https://doi.org/10.1128/JB.181.22.6865-6875.1999>
36. Gan L, Chen S, Jensen GJ. Molecular organization of Gram-negative peptidoglycan. *Proc Natl Acad Sci*. 2008; 105(48): 18953–7. <https://doi.org/10.1073/pnas.0808035105>
37. Mohamed RR, Elella MHA, Sabaa MW. Cytotoxicity and metal ions removal using antibacterial biodegradable hydrogels based on N-quaternized chitosan/poly (acrylic acid). *Int J Biol Macromol*. 2017; 98: 302–13. <https://doi.org/10.1016/j.ijbiomac.2017.01.107>

## دراسة تأثير الجسيمات النانوية لأوكسيد القصدير النقي والمخدر بالنحاس المحضر بطريقة التخليق الحيوي على النشاط البكتيري

ندى خضير عباس<sup>1</sup>، ضحى سعد شاكر<sup>2</sup>

<sup>1</sup>القسم الفيزياء، الكلية العلوم للبنات، جامعة بغداد، بغداد، العراق.

<sup>2</sup>جامعة الكرخ للعلوم، بغداد، العراق.

### الخلاصة

في هذه الدراسة، تم تشويب جسيمات SnO<sub>2</sub> النانوية بنسبة 2٪ بالوزن من النحاس بطريقة التخليق الحيوي. تم استخدام المواد الحيوية SnCl<sub>2</sub>.2H<sub>2</sub>O و CuCl<sub>2</sub>.2H<sub>2</sub>O و ESM كأغشية قشر البيض كمواد خام. تم تلدين العينات عند 550 درجة مئوية لمدة 3 ساعات. تم الحصول على الفعالية البكتيرية ضد سلالات المكورات العنقودية الذهبية سالبة الجرام و *S. aureus* إيجابية الجرام وتنشيط أعلى لتركيزات المكورات العنقودية الذهبية من *E. coli*. تم استخدام طريقة MIC لأدنى تركيز مثبط. أظهرت نتائج XRD أن العينات تبلورت ضمن النوع رباعي الزوايا الروتيل وأن متوسط حجم البلورة لـ SnO<sub>2</sub>: Cu النقي و SnO<sub>2</sub>: Cu كان (24.2، 16.6 نانومتر) على التوالي، كذلك تم إجراء اختبارات SEM و AFM كشفت دراسات UV-vis التحليل الطيفي للانعكاس عند فجوة الطاقة لـ SnO<sub>2</sub> و SnO<sub>2</sub>: Cu 2 هو (4.30، 4.35) إلكترون فولت على التوالي، وأظهرت نتائج AFM معدل الخشونة للعينات المحضرة حيث كان (9.13، 6.34) نانومتر على التوالي. كما تم إجراء فحص الـ EDX للعينات المعدة. الهدف من العمل هو إنشاء جزيئات نانوية SnO<sub>2</sub> نقية من خلال التخليق الحيوي النشط ودراسة تأثير تعاطي المنشطات بـ Cu ودراسة تأثيرها على خواصها التركيبية والبصرية وإيضاً في كيفية استخدامها كمضاد بكتيري.

**الكلمات المفتاحية:** ESM، *S. aureus* و *E. coli*، طريقة MIC، التخليق الحيوي SnO<sub>2</sub>، تركيب SnO<sub>2</sub>: Cu، SnO<sub>2</sub>.